Selective retina therapy enhanced with optical coherence tomography for dosimetry control and monitoring: a proof of concept study

DANIEL KAUFMANN,[1] CHRISTIAN BURRI,[2] PATRIK ARNOLD,[2] VOLKER M. KOCH,[1,3] CHRISTOPH MEIER,[2,4] BORIS POVAŽAY,[2] AND JÖRN JUSTIZ[1]

[1]*Bern University of Applied Sciences, HuCE BME Lab, BFH-TI, CH-2501 Biel, Switzerland*
[2]*Bern University of Applied Sciences, HuCE optoLab, BFH-TI, CH-2501 Biel, Switzerland*
[3]*volker.koch@bfh.ch*
[4]*christoph.meier@bfh.ch*

Abstract: Selective treatment of the retinal pigment epithelium (RPE) by using short-pulse lasers leads to a less destructive treatment for certain retinal diseases in contrast to conventional photocoagulation. The introduction of selective retina therapy (SRT) to clinical routine is still precluded by the challenges to reliably monitor treatment success and to automatically adjust dose within the locally varying therapeutic window. Combining micrometer-scale depth resolving capabilities of optical coherence tomography (OCT) with SRT can yield real-time information on the laser-induced changes within the RPE after a laser pulse or even during treatment with a laser pulse train. In the present study, SRT and OCT were combined to treat ex-vivo porcine eyes demonstrating closed-loop dose-control. We found a reliable correlation of specific signal changes in time resolved OCT images and physiological lesions in the RPE. First experiments, including 23 porcine eyes, prove the feasibility of the novel treatment concept.

References and links

1. G. Meyer-Schwickerath, "Light coagulation; a method for treatment and prevention of the retinal detachment," Albrecht von Graefe's Archiv fur Ophthalmologie **156**, 2–34 (1954).
2. Q. Mohamed, M. C. Gilles, and W. Ty, "Management of diabetic retinopathy: A systematic review," JAMA **298**, 902–916 (2007).
3. T. E. T. D. R. S. R. Group, "Photocoagulation for diabetic macular edema: Early Treatment Diabetic Retinopathy Study report no. 4," Int. Ophthalmol. Clin. **27**, 265–272 (1987).
4. M. P. S. Group, "Laser photocoagulation of subfoveal neovascular lesions of age-related macular degeneration," Arch. Ophthalmol. **111**, 1200–1209 (1993).
5. M. P. S. Group, "Laser photocoagulation for juxtafoveal choroidal neovascularization. Five-year results from randomized clinical trials," Arch. Ophthalmol. **112**, 500–509 (1994).
6. M. P. S. Group, "Argon laser photocoagulation for neovascular maculopathy. Five-year results from randomized clinical trials," Arch. Ophthalmol. **109**, 1109–1114 (1991).
7. G. Virgili and A. Bini, "Laser photocoagulation for neovascular age-related macular degeneration," Cochrane Database of Systematic Reviews p. CD004763 (2007).
8. I. Kozak and J. K. Luttrull, "Modern retinal laser therapy," Saudi Journal of Ophthalmology **29**, 137–146 (2015).
9. J. H. Locke and K. C. Fong, "An update on retinal laser therapy," Clinical and Experimental Optometry **4**, 43–51 (2010).
10. C. Framme, A. Walter, L. Berger, P. Prahs, C. Alt, D. Theisen-Kunde, J. Kowal, and R. Brinkmann, "Selective Retina Therapy in Acute and Chronic-Recurrent Central Serous Chorioretinopathy," Ophthalmologica **234**, 177–188 (2015).
11. T. A. Ciulla, A. G. Amador, and B. Zinman, "Diabetic retinopathy and diabetic macular edema," Diabetes Care **26**, 2653–2664 (2003).
12. Macular Photocoagulation Study Group, "Laser photocoagulation of subfoveal neovascular lesions in age-related macular degeneration: results of a randomized clinical trial," Arch. Ophthalmol. **109**, 1220–1231 (1991).
13. S. K. Houston, C. C. Wykoff, A. M. Berrocal, D. J. Hess, and T. G. Murray, "Lasers for the treatment of intraocular tumors," Lasers in Medical Science **28(3)**, 1025–1034 (2013).

14. E. Stefánsson, R. Machemer, E. de Juan, B. W. McCuen, and J. Peterson, "Retinal oxygenation and laser treatment in patients with diabetic retinopathy," American Journal of Ophthalmology **113(1)**, 36–38 (1992).

15. E. Stefánsson, "The therapeutic effects of retinal laser treatment and vitrectomy. A theory based on oxygen and vascular physiology," Acta Ophthalmologica Scandinavica **79**, 435–440 (2001).

16. E. Stefánsson, "Oxygen and diabetic eye disease," Graefe's Archive for Clinical and Experimental Ophthalmology **228(1)**, 120–123 (1990).

17. M. B. Landers, E. Stefánsson, and M. L. Wolbarsht, "Panretinal photocoagulation and retinal oxygenation," Retina **2**(3), 167–175 (1982).

18. J. E. Grunwald, C. E. Riva, A. J. Brucker, S. H. Sinclair, and B. L. Petrig, "Effect of panretinal photocoagulation on retinal blood flow in proliferative diabetic retinopathy," Ophthalmology **93**(5), 590 (1986).

19. C. Framme, G. Schuele, J. Roider, R. Birngruber, and R. Brinkmann, "Influence of pulse duration and pulse number in selective RPE laser treatment," Lasers in Surgery and Medicine **34**, 206–215 (2004).

20. O. Strauss, "The retinal pigment epithelium in visual function," Physiol. Rev. **85**, 845–881 (2005).

21. M. F. Marmor and T. Wolfensberger, "The retinal pigment epithelium," in *Function and Disease* (Oxford, 1998), pp. 103–134.

22. L. V. Del Priore, B. M. Glaser, H. A. Quigley, and W. R. Green, "Response of pig retinal pigment epithelium to laser photocoagulation in organ culture," Arch. Opthamol. **107**, 119–122 (1989).

23. J. Roider, N. Michaud, T. Flotte, and R. Birngruber, "Histology of retinal lesions after continuous irradiation and selective micro-coagulation of the retinal pigment epithelium," Ophthalmologe **90**(3), 274–278 (1993).

24. G. H. Bresnick, "Diabetic maculopathy: a critical review highlighting diffuse macular edema," Ophthalmology **90**, 1301–1317 (1983).

25. C. Klatt, M. Saeger, T. Oppermann, E. Pörksen, F. Treumer, J. Hillenkamp, E. Fritzer, R. Brinkmann, R. Birngruber, and J. Roider, "Selective retina therapy for acute central serous chorioretinopathy," British Journal of Ophthalmology **95**, 83–88 (2010).

26. J. Roider, S. H. M. Liew, C. Klatt, H. Elsner, E. Poerksen, J. Hillenkamp, R. Brinkmann, and R. Birngruber, "Selective retina therapy (SRT) for clinically significant diabetic macular edema," Graefe's Archive for Clinical and Experimental Ophthalmology **248**, 1263–1272 (2010).

27. Y. G. Park, J. R. Kim, S. Kang, E. Seifert, D. Theisen-Kunde, R. Brinkmann, and Y.-J. Roh, "Safety and efficacy of selective retina therapy (SRT) for the treatment of diabetic macular edema in Korean patients," Graefe's Archive for Clinical and Experimental Ophthalmology **254**, 1703–1713 (2016).

28. J. Roider, R. Brinkmann, C. Wirbelauer, H. Laqua, and R. Birngruber, "Subthreshold (retinal pigment epithelium) photocoagulation in macular diseases: a pilot study," British Journal of Ophthalmology **84**, 40–47 (2000).

29. C. Framme, R. Brinkmann, R. Birngruber, and J. Roider, "Autofluorescence imaging after selective RPE laser treatment in macular diseases and clinical outcome: a pilot study," British Journal of Ophthalmology **86**, 1099–1106 (2002).

30. R. Brinkmann, J. Roider, and R. Birngruber, "Selective retina therapy (SRT): a review on methods, techniques, preclinical and first clinical results," Bulletin De La Societe Belge D'Ophtalmologie **302**, 51–69 (2006).

31. J. Roider, F. Hillenkamp, T. Flotte, and R. Birngruber, "Microphotocoagulation: selective effects of repetitive short laser pulses," Proceedings of the National Academy of Sciences **90**, 8643–8647 (1993).

32. V.-P. Gabel, R. Birngruber, and F. Hillenkamp, "Visible and near infrared light absorption in pigment epithelium and choroid," *Proc. 23rd Consilium Ophthalmologicum, (Kyoto)* Excerpta Medica (1978), pp. 658–662.

33. V. Chichagova, D. Hallam, J. Collin, D. Zerti, B. Dorgau, M. Felemban, M. Lako, and D. H. Steel, "Cellular regeneration strategies for macular degeneration: past, present and future," Eye **32**, 946 (2018).

34. J. Neumann and R. Brinkmann, "Nucleation and Dynamics of Bubbles Forming Around Laser Heated Microabsorbers," Optical Society of America (2005).

35. R. Brinkmann, G. Huettmann, J. Roegener, J. Roider, R. Birngruber, and C. Lin, "Origin of retinal pigment epithelium cell damage by pulsed laser irradiance in the nanosecond to microsecond time regimen," Lasers in Surgery and Medicine **27**, 451–464 (2000).

36. G. Schuele, M. Rumohr, G. Huettmann, and R. Brinkmann, "RPE damage thresholds and mechanisms for laser exposure in the microsecond-to-millisecond time regimen," Investigative Ophthalmology & Visual Science **46**, 714–719 (2005).

37. J. Neumann and R. Brinkmann, "Microbubble dynamics around laser heated microparticles," Proc. SPIE **5142**, 82–87 (2003).

38. C. Framme, G. Schuele, J. Roider, D. Kracht, R. Birngruber, and R. Brinkmann, "Threshold determinations for selective retinal pigment epithelium damage with repetitive pulsed microsecond laser systems in rabbits," Ophthalmic Surgery, Lasers **33**, 400–409 (2002).

39. C. Framme, A. Walter, P. Prahs, D. Theisen-Kunde, and R. Brinkmann, "Comparison of threshold irradiances and online dosimetry for selective retina treatment (SRT) in patients treated with 200 nanoseconds and 1.7 microseconds laser pulses," Lasers in Surgery and Medicine **40**, 616–624 (2008).

40. S. Y. Schmidt and R. D. Peisch, "Melanin concentration in normal human retinal pigment epithelium. Regional variation and age-related reduction," Investigative Ophthalmology & Visual Science **27**, 1063–1067 (1986).

41. A. Yasui, M. Yamamoto, K. Hirayama, K. Shiraki, D. Theisen-Kunde, R. Brinkmann, Y. Miura, and T. Kohno, "Retinal sensitivity after selective retina therapy (SRT) on patients with central serous chorioretinopathy," Graefe's

Archive for Clinical and Experimental Ophthalmology **255**, 243–254 (2017).

42. S. Muhammad, "Fundus Fluorescein Angiography," Journal of Postgraduate Medical Institute (Peshawar - Pakistan) **12**, 1 (2011).

43. E. Seifert, Y.-J. Roh, A. Fritz, Y. G. Park, S. Kang, D. Theisen-Kunde, and R. Brinkmann, "Automatic irradiation control by an optical feedback technique for selective retina treatment (SRT) in a rabbit model," in "European Conferences on Biomedical Optics," (International Society for Optics and Photonics, 2013), pp. 880303.

44. Y.-G. Park, E. Seifert, Y. J. Roh, D. Theisen-Kunde, S. Kang, and R. Brinkmann, "Tissue response of selective retina therapy by means of a feedback-controlled energy ramping mode," Clinical & Experimental Ophthalmology **42**, 846–855 (2014).

45. G. Schuele, M. Rumohr, G. Huettmann, and R. Brinkmann, "RPE damage thresholds and mechanisms for laser exposure in the microsecond-to-millisecond time regimen," Investigative Ophthalmology & Visual Science **46**, 714–719 (2005).

46. W. Drexler and J. G. Fujimoto, *Optical Coherence Tomography: Technology and Applications* (Springer Science & Business Media, 2008).

47. K. Bizheva, B. Tan, B. MacLelan, O. Kralj, M. Hajialamdari, D. Hileeto, and L. Sorbara, "Sub-micrometer axial resolution OCT for in-vivo imaging of the cellular structure of healthy and keratoconic human corneas," Biomedical Optics Express **8**, 800–812 (2017).

48. P. Steiner, A. Ebneter, L. E. Berger, M. Zinkernagel, B. Považay, C. Meier, J. H. Kowal, C. Framme, R. Brinkmann, S. Wolf, and R. Sznitman, "Time-Resolved Ultra–High Resolution Optical Coherence Tomography for Real-Time Monitoring of Selective Retina TherapyTime-Resolved Ultra–High Resolution OCT During SRT," Investigative ophthalmology & visual science **56**, 6654–6662 (2015).

49. C. Framme, A. Walter, P. Prahs, R. Regler, D. Theisen-Kunde, C. Alt, and R. Brinkmann, "Structural changes of the retina after conventional laser photocoagulation and selective retina treatment (SRT) in spectral domain OCT," Current eye research **34**, 568–579 (2009).

50. K. Kurokawa, S. Makita, and Y. Yasuno, "Investigation of thermal effects of photocoagulation on retinal tissue using fine-motion-sensitive dynamic optical coherence tomography," PloS one **11**, e0156761 (2016).

51. H. H. Müller, L. Ptaszynski, K. Schlott, C. Debbeler, M. Bever, S. Koinzer, R. Birngruber, R. Brinkmann, and G. Hüttmann, "Imaging thermal expansion and retinal tissue changes during photocoagulation by high speed OCT," Biomedical optics express **3**, 1025–1046 (2012).

52. D. Kaufmann, C. Burri, P. Arnold, V. M. Koch, C. Meier, B. Považay, and J. Justiz, "Dosimetry control and monitoring of selective retina therapy using optical coherence tomography," Proc.SPIE **10416**, 10416–10416–6 (2017).

53. P. Steiner, "Ultra-high Resolution Optical Coherence Tomography Retinal Tissue Monitoring for Dosimetry Control during Selective Retina Therapy Laser Treatment," Ph.D. thesis, Graduate School for Cellular and Biomedical Sciences University of Bern (2015).

54. Y. M. Paulus, A. Jain, H. Nomoto, C. Sramek, R. F. Gariano, D. Andersen, G. Schuele, L.-S. Leung, T. Leng, and D. Palanker, "Selective retinal therapy with microsecond exposures using a continuous line scanning laser," Retina **31**, 380–388 (2011).

55. J. N. Crosson, L. Mason, and J. O. Mason, "The role of focal laser in the anti–vascular endothelial growth factor era," Ophthalmology and eye diseases **9**, 1179172117738240 (2017).

1. Introduction

While already in the 1950s panretinal photocoagulation (PRP) using xenon arc lamps were employed for sealing retinal breaks and treating tumors [1] the actual break-through of PRP only occurred with the advent of lasers in the 1960s that allowed precise focusing of high energy beams. Guided by slit-lamps, lasers reduced the spot-size on the retina from 2000 µm to 100 µm. Increased focus ability and energy density allowed ophthalmologists to apply the treatment in a much more precise way. These laser photocoagulation (LPC) techniques were shown to be effective therapies for proliferative diabetic retinopathy [2] and advanced forms of nonproliferative diabetic retinopathy associated with macular edema [3]. Later, LPC was also proposed for the treatment of age related macular degeneration (AMD) and other macular diseases [4–7]. Today, LPC still remains an established method for retinal diseases. Progress in real-time visualization technologies like fundus cameras, confocal retinal laser scanners and even 3D-imaging like optical coherence tomography further improve the procedure.

The underlying mode of action for photocoagulation relies on the thermal destruction of retinal cells due to absorption of laser light directed through the eye. The rise in local temperature of 20°C to 30°C, by heating of the intracellular melanosome, causes denaturation of the heated proteins and cauterizes vessels and the overlying photoreceptors by heat diffusion [8–10]. Due

to the slow heating process and the strong heat dissipation into the surroundings, before local temperature can rise, the use of long laser pulses (~ms) or even continuous wave lasers risks to destroy cells in all retinal layers and laterally neighbored regions, impairing healthy photoreceptor (PR) cells [11, 12]. These adverse effects can lead to scotomata, reduced night vision, and disruption of the retinal anatomy through scarring.

LPC's ability to destroy tissue that does not directly absorb the radiation can be utilized to deactivate unhealthy tissue such as tumors [13]. Furthermore, it was shown that LPC can also be used to increase oxygen and nutrient supply to the inner retina, thus favorably altering the hemodynamics [14, 15]. Different hypotheses explaining this process have been developed, including laser-disruption of tight junctions in the retinal pigment epithelium (RPE), increased inward oxygen diffusion [16] and reduction of oxygen demand of outer retina layers followed by increased oxygen and nutrient supply to the inner retina due to the destruction of energy-demanding tissue [16–18]. As the RPE layer between retina and choroid is part of the blood-brain barrier, it controls permeability between the photosensitive tissue of the retina and the nutrient- and oxygen-rich choroid as well as the active transport through these regions [19, 20]. Like other epithelia it also can completely regenerate through cellular proliferation after damage from healthy regions, which is unique amongst all retinal layers [21, 22]. Restoration of the RPE after laser treatment has been documented histologically, which may be explained by the establishment of a new barrier of RPE cells and a subsequent re-activation of the RPE pump and thus providing the RPE's integrity [23, 24]. This has led to the development of a new form of treatment that deposits energy primarily in the RPE, the so-called selective retina therapy (SRT). SRT demonstrated successful treatment of central serous chorioretinopathy (CSC), diabetic macular edema (DME) and AMD [25–30]. Selective treatment of the RPE layer is enabled by the high melanin concentration within the ~10 μm thick monolayer, which absorbs about 50% of the incident radiation across a wide spectrum spanning from the UV to the near infrared [31]. During normal vision this enables the RPE to prevent diffuse scattering and multiple detection of light by the more superficial photoreceptors, which would result in image blur [20, 32]. The only regenerative PR-portion, the outer segments, interdigitate with the apical microvilli of the RPE, which facilitates selective heating of the RPE.

An aging Bruch's membrane (BM) has been identified as a potential cause for numerous diseases and in fact might be the physiological target of the SRT treatment. Due to the lack of a widely approved working mechanism for SRT, our working hypothesis is that selective destruction, removal and regrowth or transplantation of the dysfunctional RPE-BM-choriocapillaris (CC)-complex, which results in a local rejuvenation, builds the basis for treatment of multiple diseases [33].

The performance of SRT relies on spatial and temporal confinement which reduces the energy required to achieve the same result without affecting neighbored layers when the laser operates with a pulse length shorter than the thermal relaxation time of the RPE of 10 μs [30]. During this process, the structural integrity of RPE cells is destroyed by fast expanding and collapsing microbubbles which are formed around laser heated intracellular pigments [34–36]. Although the precise biological effects, especially caused by sub-lethal cellular irradiation, still need to be evaluated clinically, it is certain that cell-wall rupture leads to cell death.

Since SRT ideally only affects the RPE, it is much less destructive than conventional photocoagulation and leaves the original layered morphology intact. Henceforth proper control of pulse energy and pulse duration is crucial to introduce therapeutically significant lesions in the RPE to limit collateral damage by excess energy deposition [37–39]. Since absorption properties vary significantly and non-predictively between eyes and even within the same eye on cellular level [32, 40], it is impossible to set a static threshold value for the optimum pulse energy that always fits the local therapeutic window. Ophthalmoscopically, lesions in the RPE are invisible and in practice only detectable two hours after treatment through fundus fluorescence

angiography (FFA) [31, 41]. As the perforations in the RPE leak blood through the locally interrupted blood-brain barrier, FFA shows this bleeding on the retinal side of the RPE-CC-complex and clearly demarks successfully treated RPE sites [42]. While very accurate, the long delay between treatment and detection as well as side-effects evoked by the injected dye limit the usefulness of FFA in medical routine and prevent practicable simultaneous monitoring of SRT performance within a single session.

For real-time feedback on treatment success, several approaches are taking advantage of microbubbles generation and also of the associated shock-wave that is emitted during their expansion and collapse. Methods such as measuring the change in reflectivity at the bubble surface with backscattered light have been implemented [43,44]. It was found that the backscattered light changes as soon as microbubbles appear. First studies with chinchillas showed a good match in general when comparing the signal difference of the emitted pulse and the backreflected light, which is higher in the case of microbubbles, with the gold standard evaluation methods like fluorescine angiography, fundus photography, OCT and histology. Another real-time dosimetry approach uses the acoustic feedback to detect the appearance of microvapour bubbles [36, 43, 44]. During μs laser treatment, optoacoustic transients are induced at the RPE. The characteristic of the acoustic signal strongly changes due to the fast volume change as soon as micro bubble grow and collapse [45]. Therefore, this method needs calibration with low energy treatment pulses. The complexity involved prohibited wide uptake of the technology and did not allow to establish SRT as standard therapy for the above mentioned retinal diseases.

Here we describe the use of real-time optical coherence tomography (OCT) in parallel to SRT to observe signal variations correlated to the creation of RPE lesions. OCT is a spectrally broadband, depth resolving and successively cross-sectional imaging technique based on low-coherence interferometry [46]. As a fast (~10 kHz), non-invasive and non-contact technique it is already well established for high-resolution optical recording of the three-dimensional reflectivity in long term changes [46]. Modern OCT systems are able to resolve axial structures of typically 1 μm to 10 μm in-vivo and even systems with axial resolutions in the sub-micrometer range have been reported [47].

With this method we follow up on [48] where effects of treatment laser pulses could be indirectly detected as a change of intensity of the OCT depth-scans (A-scans), which correspond to the local reflectivity of tissue. In a time-resolved sequence of A-scans, an M-scan (motion mode), the change in the complex pattern is seen as an obvious interruption. While several groups used OCT as imaging modality to compare layers before and after treatment [49, 50], or Doppler OCT for thermal expansion measurements [51], Steiner et al. have been, to our knowledge, the only ones using OCT for real-time SRT quantification of the direct shock-wave formation.

Pursuing their work, we show in this more extensive study, that the signal changes in OCT M-scans during SRT allow precise real-time prediction of retinal lesions. In combination with adaptive laser pulse energy, using SRT in ramp-mode, and a fast algorithm-based treatment stop, OCT-SRT can provide a reliable dosimetry control during treatment.

2. Materials and methods

For this study, ex-vivo porcine eyes were collected at a local slaughterhouse, transported in cooled saline solution and treated within three hours post-mortem. Out of 29 treated eyes with 1421 treatment spots, 23 eyes and 1054 treatment spots were included. Six eyes and a total of 367 treatment spots were excluded because an evaluation was not possible (mostly because of damage of the RPE during the preparation for live/death staining). To maintain stable physiological conditions, the cornea was regularly humidified during treatment. Our experimental setup consisted of a medically approved commercial SRT treatment system (R:Gen; Lutronic, Goyang, Republic of Korea) and an in-house built OCT system. The narrowband, multimode treatment laser operated at 527 nm wavelength, 1.7 μs pulse length and with adjustable pulse

energies between 13 μJ and 340 μJ. On the retina, a spot size of 160 μm was reached with a top hat beam shape. A pulse train of 30 pulses at 100 Hz was shot during treatment. R:Gen's "ramp mode", which increased energy linearly from pulse to pulse with minimum energy set to 39.4 μJ and maximum to 197 μJ (see Fig. 1 for illustrations), was used.
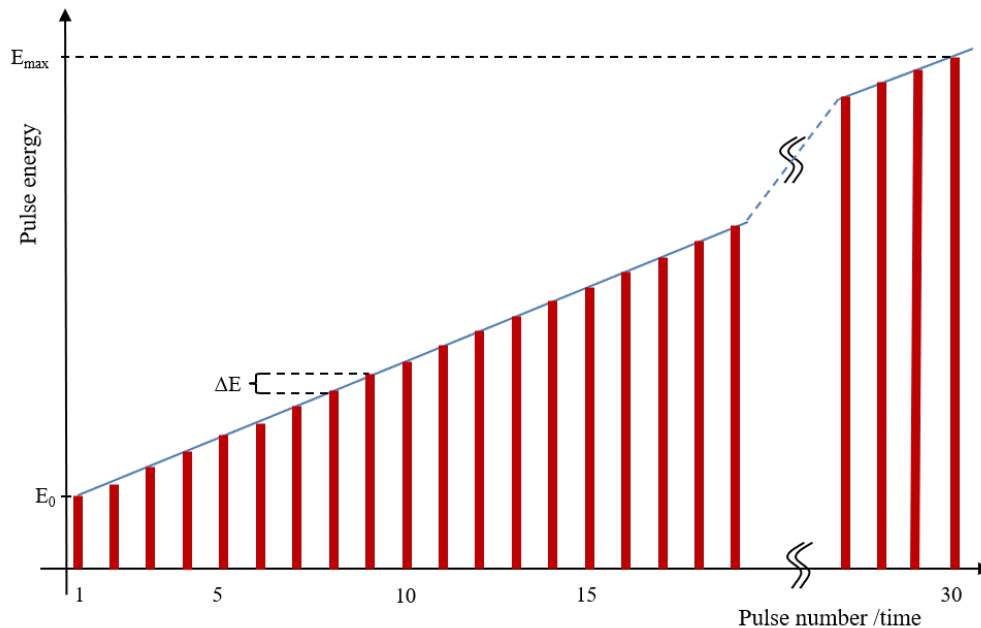

Fig. 1. In *ramp mode* the pulse energy increases from pulse to pulse within one pulse train. By adjusting the trigger signal length, the number of pulses and thus the maximum applied energy can be adjusted.

To alter the last applied pulse energy although the maximum energy E_{max} remained fixed, the trigger signal length for the treatment laser was modified to fire either only the first pulse, the first 4, 9, 14, 18, 23 or all 30 pulses (in which case E_{max} was reached). Previous work, in which a pulse repetition rate of 100 Hz was used, has shown that each pulse within one burst can be considered as standalone because no significant cumulative effects take place [52]. The seven different burst lengths correspond to seven different classes and were evaluated as such, as can be seen in Table 1. Low-power treatment positions on the RPE were hard to identify individually under the microscope. A predefined pattern, as shown in Fig. 4(b), was marked using high energy marker lesions. A scanhead using mirrors in two axes allowed directing the focus of both beams simultaneously. The OCT system uses a broadband light source (Exalos, Switzerland) with a central wavelength of λ_C = 800 nm, $\Delta\lambda$ = 120 nm of spectral bandwidth, a CCD line camera (AVIIVA EM4, ev2, UK) with 2048 pixels as parts of an in-house developed spectrometer. An overall sensitivity of ~100 dB was achieved, which is sufficient to identify and track the retinal layers of interest and is typical for commercial ophthalmic OCT devices. The beams of the treatment laser and the OCT laser were aligned coaxially in free space using a dichroic 700 nm long-pass mirror so that the OCT-scan contained the center of the therapeutic laser as shown in Fig. 2. Eyes were treated at 49 different locations while OCT signals were recorded at an amplitude mode scan (A-scan) rate of 50 kHz during each 300 ms long treatment cycle focused on the RPE. A-scans were arranged sequentially to yield a time modulated, depth-resolved image or M-scan [53].
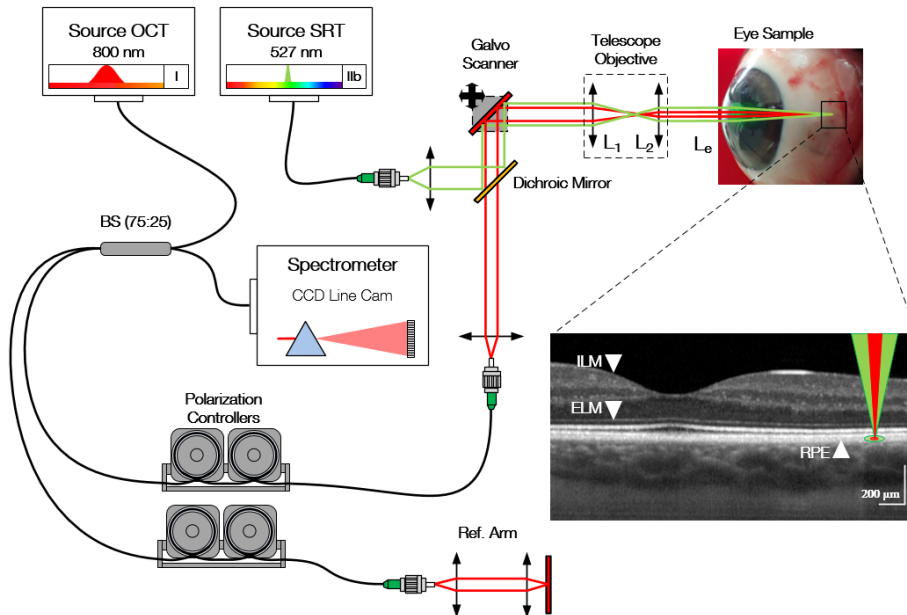
Fig. 2. Setup of the combined collinear SRT- and OCT system. BS: Beam splitter, with 75:25 ratio, where 75 % of incident light is conducted into the sample arm. Ref. Arm: Reference arm, in free-space and with the possibility to change polarization via manual fiber polarization controllers. To prevent polarization-caused transmission proprieties changes in the dichroic mirror, identical polarization controllers are inserted into the sample arm. L_1 and L_2 constitute the delivery optics that enable scanning and positioning of the laser beam within the eye by using the scanhead. L_e is the lens of the eye itself. Therapy laser and OCT laser are focused on the retina. Reflected light is separated again by the dichroic mirror. Interfering light (from sample and reference arm) covering the 120 nm bandwidth is expanded by a spectrometer and finally analyzed by a CCD line cam.

2.1. Biological evaluation using live/dead staining

Immediately after treatment, eyes were cut open posterior to the lens in the coronal plane. The vitreous body was removed, the upper retinal layers were peeled off, in order to have direct vision on the RPE, that typically stays attached to the CC in the rigid part of the sample, containing the sclera and choroid. The region of interest was cut out, resulting in a block of approximately 7 mm × 7 mm with the thickness of the sclera and choroid. The LIVE/DEAD Viability/Cytotoxicity Kit L3224 (Invitrogen, Paisley, UK) was used to mark living and dead cells, according to its protocol. Evaluation took place utilizing a Zeiss Axio Lab.A1 (Zeiss, Germany) fluorescence microscope with 470 nm excitation frequency and the Zeiss FS 56HE filters. Calceine, emitting at 517 nm binds to living cells, which appeared green under the fluorescence microscope, while ethidium homodimer can penetrate the cell wall of dead cells and binds to the DNA in the nuclei, which then appeared as red dots (Fig. 3) [54]. Directly visible thermo-mechanical cellular damage and short-term cell death until fixation was therefore defined as the pass-fail criterion. Long term cellular or tissue changes and the differentiation between apoptosis and necrosis would require live animal treatment or culturing of the enucleated eye, which was not the aim of the current study.
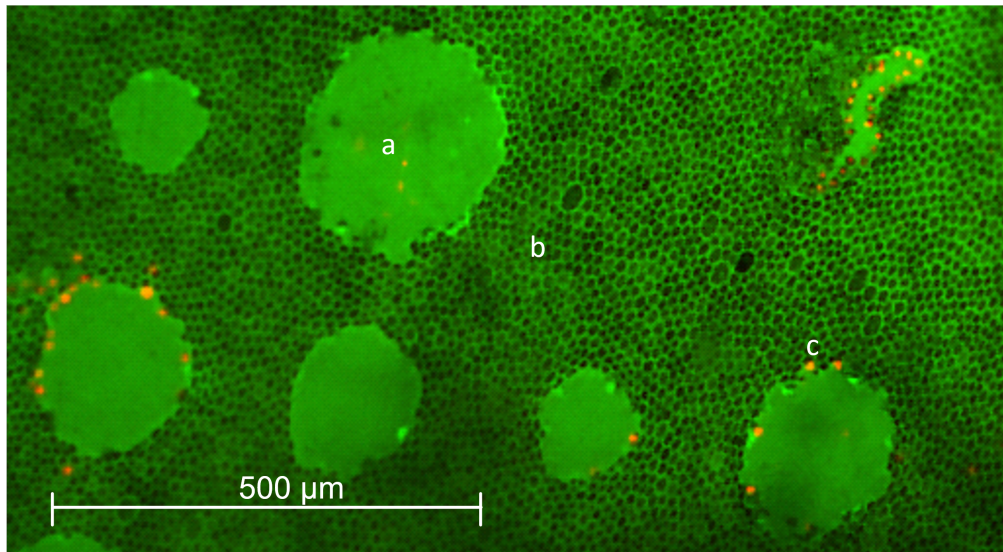
Fig. 3. Fluorescence microscope image of the scleral sample portion after peeling of the inner retina, viewed from the retinal side. Cells were stained 5 hours post mortem. At sites of treatment (Region a), the typically hexagonal arranged isoprismatic RPE cells disappeared completely and single dead cells can be seen as red dots at lesion borders (Region c). Region b shows healthy living cells.

2.2. Manual and automated M-scan signal washout detection

Evaluation of the recorded OCT M-scans took place post-treatment. Typical M-scans can be seen in Fig. 4(a). The single most striking feature during laser exposure is a sudden drop in OCT A-scan signal strength, where reflectivity information suddenly completely disappears. The origin of this missing OCT-signal will be discussed below.

For every applied treatment location, the corresponding M-scan was analyzed for signal washout. An M-scan was labeled *positive* in case of these visible signal washouts predicting a lesion in the RPE layer. Conversely, no visible signal washout meant a *negative* label for the M-scan, hence predicting no lesion. All M-scans were visually inspected by the investigators. The investigator labeled each M-scan accordingly. Additionally, the algorithm described below has been developed in order to detect these signal washouts in an automated manner, as it was planned to be implemented for further studies or later in clinics. To establish the algorithm, the results of the manual evaluation were used as the gold standard.

The first step of the algorithm was to detect the retinal pigment epithelium. This layer had the highest intensity, hence the highest pixel values in the image. To detect the signal washouts, which are characterized by vertical edges, a continuous Sobel-operator, as a standard edge detection filter, was applied. After filtering, the pixel-values of each A-scan were added, scaled and stored (X). To detect signal washout, the algorithm moved from left to right through the M-scan image (compare Fig. 5). It compares the value X of the current A-scan with a current threshold value (CTh). If X is above the threshold, a signal washout is detected and the A-scan was labeled as *positive*, meaning it contained a signal washout. The threshold was not static because M-scan appearance is changing from each recording to another, therefore the threshold was calculated according to (1). The threshold is calculated using the 50 A-scans recorded immediately before the current A-scan. The current mean value of the filter ($\bar{X}$) is used to give the baseline of the threshold while the current standard deviation (σ_n) and a sensitivity factor (κ) is used to adapt the

filter to noise. In case of large noise, the standard deviation increases and therefore the threshold gets higher to reduce the number of also positives.

$$\text{CTh} = \bar{X} + \sigma_n \times \kappa \tag{1}$$

$$\bar{X} = \frac{1}{50} \sum_{n-50}^{n-1} X \tag{2}$$

$$\sigma_n = \sigma(\{X_{n-50}, ..., X_{n-1}\}) \tag{3}$$

with:
CTh = current threshold
X = cumulative sum A-scan after edge detection
$\bar{X}$ = current mean value of the filter
σ_n = current standard deviation
κ = sensitivity factor

The sensitivity factor value was trained on separate data to obtain the best fit with the gold standard.

3. Results and discussion

3.1. Origin of the OCT signal washout and speckle variations

Obviously, the simplest assumption for explaining the temporary disappearance as due to a suddenly diminished tissue reflectivity does not apply. Also, overexposure of the spectral filter detector is not applicable because of the spectrally well separated excitation laser. Following the model of a higher reflective gas-bubble, which is supported by direct reflectivity measurements, the increase of reflected light can lead to saturation of the OCT's sample arm signal, followed by a lack of spectral modulation that is the carrier of depth information within the frequency domain encoded reflectivity measurement. However, an increase of reflectivity and saturation of the spectrum is not visible in the underlying spectra. As a third explanation rapid changes in the spectral signal can cause fringe-washout in the time-integrating spectrally resolving OCT-sensor. Especially the occurrence of a highly reflective bubble, but still with less than 8% of reflectivity and a bent surface, can easily cast strong spectral oscillations on top of the much weaker signals from the surrounding tissue. Due to the microsecond fast expansion of the bubble in the axial resolution range the quickly changing signal would be time-integrated on the comparably slow detector, which reduces its visibility due to destructive summation. The most viable explanation for the signal loss is a fringe-washout caused by the mechanical vibrations due to rapid expansion of the bubble. Fringe-washout requires a phase-shift larger than $\pi/2$ or a physical shift of more than half the carrier wavelength within a single acquisition and can be simulated by vibration of tissue. To avoid this signal loss due to an acoustic shock-wave, OCT sampling frequencies above 100 MHz or exposure times < 10 ns would be required. Sound waves in tissue travel at more than 1000 m s^{-1} and the reflections from the rapidly shifted material (> 10 modulations during a single A-scan acquisition time-window) within the depth-scan create the effect already described above. Here however, the full depth-scan is suppressed, which perfectly corresponds to the measurements.
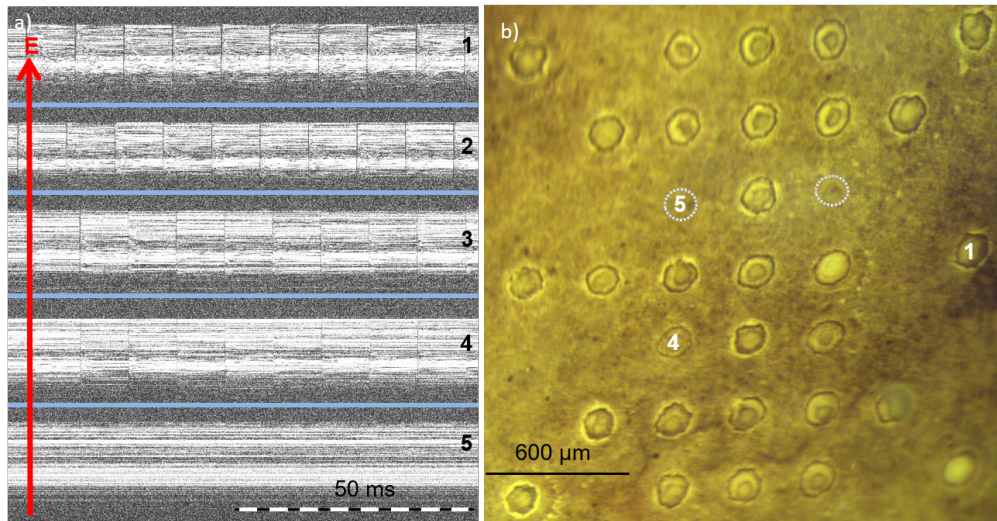
Fig. 4. a) M-scans from treatments using *classic mode* (all pulses with the same energy). The red arrow indicates the pulse energy level, which increases from M-scan number 5 to M-scan number 1. In the lowest energy M-scan (number 5) no apparent signal washout is visible while the M-scan with highest pulse energy (number 1) shows distinct signal washouts. b) Top view onto RPE layer under bright field microscope. The applied treatment pattern is visible and allows for easy location of the treatment positions. Strong lesions, such as lesion number 1, relate to strong signal washouts in the corresponding M-scan (M-scan number 1). Weak lesions (e.g., lesion number 4) conversely relate to weak M-scan signal washouts. Spots with no visible lesion in the RPE layer (e.g., spot number 5) correlate to M-scans without any signal washout.

Slower propagating effects, such as heat diffusion, were responsible for the temporal expansion in signal washouts and shifts and speckle-changes that can be recognized in the M-scans. Clearly, these effects were more pronounced for pulses with higher laser energies as depicted in Fig. 5(b). This relationship could be exploited to relate the emerging signal washouts to the destruction of RPE cells. Apparently, primarily cells that were destroyed by mechanical rupture due to micro-bubble formation caused enough mechanical shift for the fringe washout. A minor portion of false positives might be explained by the generation of a microbubble that was too small for cell destruction, but strong enough to generate a shock-wave that influenced the OCT-scan. In the following we empirically demonstrated this correlation.

3.2. *Live/dead staining results*

The LIVE/DEAD Viability/Cytotoxicity Kit L3224 confirmed that RPE and retinal cells were still alive longer than five hours post-mortem. An example that demonstrated this behavior is shown in Fig. 3, where most of the hexagonal RPE cells appeared in green when inking this sample five hours post-mortem. This figure also confirms spatial selectivity of the treatment within the RPE plane, as RPE cells appeared green in regions where no treatment took place (Region b in Fig. 3), and dead cells were only found in border regions of a lesion. Often, there were no RPE cells in the center of laser treatment spots because during treatment, microbubble formation led to a rupture of the cell membrane and the cell content was washed away during preparation. At locations where no laser treatment has been made, cells were found intact.

To exploit these findings, OCT M-scans have been used to predict the treatment outcome within the biological tissue. Table 1 shows the results for the M-scan evaluation by an investigator, while Table 2 show the results for the M-scan evaluation by the before described algorithm. Based
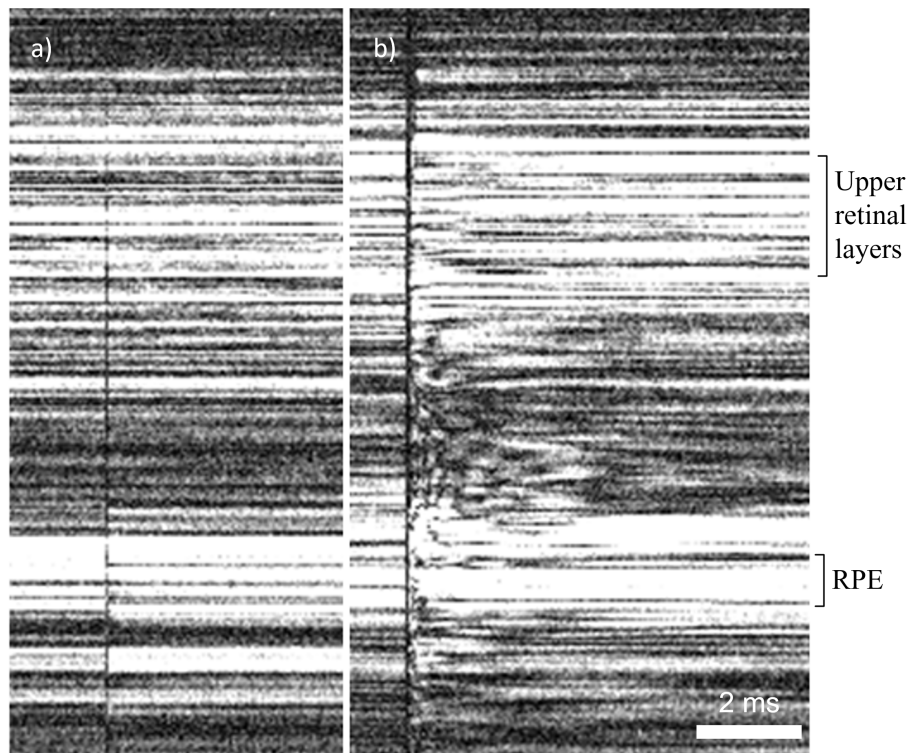
Fig. 5. Signal washouts in M-scan caused by treatment in ramp-mode. *a)* Signal washout (vertical black line) in M-scan induced by one single laser pulse with 54 μJ. *b)* Signal washout induced by one single laser pulse with pulse energy of 180 μJ. The duration of the signal washout in the upper retinal layers is longer than at the level of the RPE. Additionally, layers in the middle are distorted for a longer time (~4 ms).

on OCT M-scans, 795 treatment spots were correctly predicted by the manual evaluations, and 791 treatment spots by evaluation via algorithm (accuracy of 75 % in both cases).

The longer the chosen pulse burst, the more pulses were fired and the higher the pulse energy of the last pulse. Therefore, the probability of cell destruction by microvapour bubble increased resulting in a raise of predicted and detected lesions. With increasing treatment energy, the observed signal washouts became intenser. For moderate energies signal washouts were restricted to the RPE layer and spanned over one A-scan, as visible in Fig. 5(a). Higher energies gave rise to more intense signal washouts, like in Fig. 5(b), spanning over multiple A-Scans and thus were easier to identify. The results in Table 1 also indicate that lower treatment pulse energies can reduce the accuracy because here some optically visible lesions showed no discernible signal washout. Figure 6 shows examples of false positive and false negative results. The fluoroscopic examination showed that relatively low treatment energies killed only a few cells in the laser focal point. While these are apparently not sufficient to cause a detectable signal washout, it remains open whether these cases are indeed misclassified because to our knowledge no study has shown a minimum number of dead RPE cells necessary for a successful treatment.

Both evaluation methods were less sensitive for classes with low pulse numbers (class 1 and 4) and less specific for classes with higher pulse numbers (class 23 and 30). In the classes 1 and 4, the number of true positives and false negatives to calculate the sensitivity is very small and like-wise in classes 23 and 30, the numbers of true negatives and false positives to calculate the specificity is again very small, yielding statistically questionable results.

Table 1. Visual evaluation by an investigator. Results for the seven classes of different number of laser pulses. All were acquired using the same ramp mode but with different number of pulses.

Class (Number Pulses)	1	4	9	14	18	23	30	**Overall**
Energy of Last Pulse [μJ]	39	69	93	118	137	162	197	
Number Evaluated Spots	151	153	151	150	153	145	151	**1054**
Signal Washouts in OCT	14	51	93	115	125	129	142	**669**
Lesions in RPE*	66	115	113	142	141	141	148	**866**
Correct Predictions	95	85	97	117	131	127	143	**795**
Accuracy**	0.63	0.56	0.64	0.78	0.86	0.88	0.95	**0.75**
Sensitivity	0.18	0.43	0.67	0.79	0.87	0.89	0.95	**0.74**
Specificity	0.98	0.95	0.55	0.63	0.75	0.25	0.67	**0.84**
* Seen under the fluorescence microscope								
** Assuming the prevalence is correct, with a 95% confidence interval of [0.728, 0.780]								

Table 2. Evaluation by algorithm. Results showed for the 7 classes with different number of laser pulses. All were acquired using the same ramp mode but with different number of pulses.

Class (Number Pulses)	1	4	9	14	18	23	30	**Overall**
Energy of Last Pulse [μJ]	39	69	93	118	137	162	197	
Number Evaluated Spots	151	153	151	150	153	145	151	**1054**
Signal Washouts in OCT	36	58	97	121	129	132	140	**713**
Lesions in RPE*	66	115	113	142	141	141	148	**866**
Correct Predictions	93	74	99	121	131	132	141	**791**
Accuracy**	0.62	0.48	0.66	0.81	0.86	0.91	0.93	**0.75**
Sensitivity	0.33	0.41	0.70	0.82	0.88	0.92	0.94	**0.76**
Specificity	0.84	0.71	0.53	0.50	0.58	0.50	0.67	**0.71**
* Seen under the fluorescence microscope								
** Assuming the prevalence is correct, with a 95% confidence interval of [0.728, 0.780]								

Comparing the two tables, similar overall values for accuracy, sensitivity and specificity were found for the evaluation by hand and the evaluation by algorithm, with slightly better values for the findings by hand. In general the signal washout, as a predictor for RPE lesions, yields a sensitivity of over 76% for the algorithm and 74% for the evaluation by hand. This means that 76% and 74%, respectively, of all lesions in the RPE layer were detected as such in the M-scan evaluation. The achieved specificity was 84% and 71%, respectively. So, out of all spots treated with laser energies too low for inducting lesions, 84% and 71%, were correctly predicted as non-lesions based on M-scans as evaluated by the investigators and the algorithm, respectively.
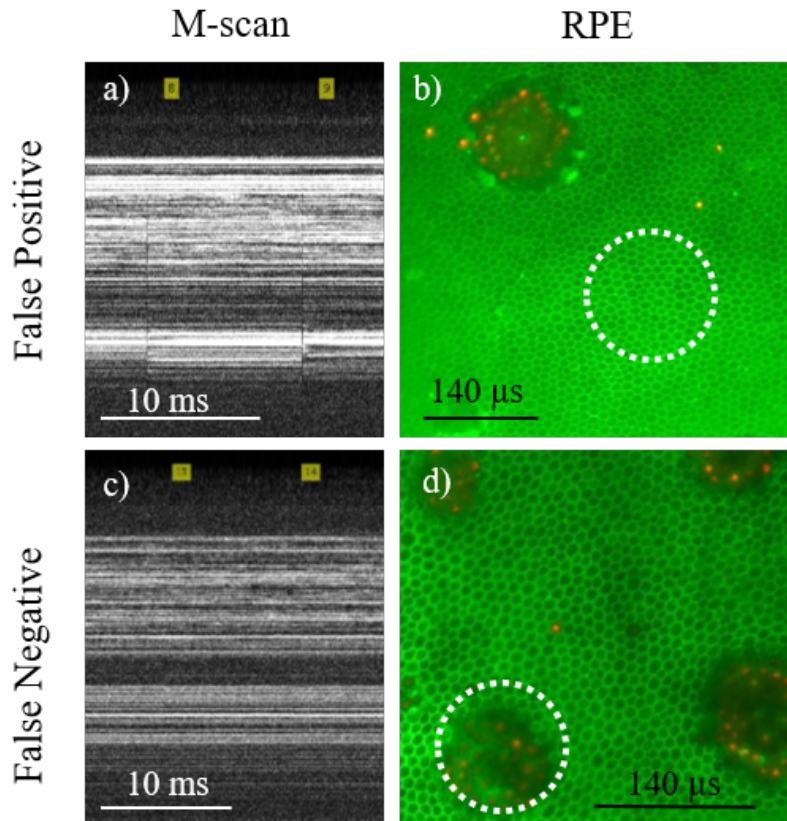
Fig. 6. This picture illustrates what is defined as *false positive* and *false negative*. Although there is no lesion in b) at the position encircled in white, the M-scan in a) shows signal washouts. In contrast, the M-scan in c) did not show any signal washout but the corresponding region, marked with a white circle, in d) shows a clear damage in the RPE cell structure.

3.3.   Opthalmologic treatment protocol

Based on our empirically established relationship between OCT signals and induced RPE lesions, we propose to simultaneously monitor SRT by OCT. In particular, the application of the following protocol will increase the reliability to obtain sufficient RPE lesions while remaining well below the threshold for destruction of the entire retina. Starting with a value guaranteed to lie below the photo-coagulation threshold, the laser's pulse-energy is successively increased in the ramp mode. An algorithm detects signal washouts as soon as they appear in the simultaneously acquired M-scan and immediately stops the SRT laser (Fig. 7).

3.3.1.   Proof of concept with manual dose control

We validated this procedure and the signal washout within OCT M-scans as predictor for SRT success manually since our detection algorithm was not yet real-time capable. Here, the investigator triggered single treatment pulses with increasing energy and checked for signal washout directly after each shot. Once a washout was visible, the treatment at the current position was stopped and the next target was treated. In the subsequent analysis as described above, the treatment success at each location was assessed.

The pulse energies chosen for this protocol fit the pulse energies of a ramp mode with a maximal energy of 197 μJ. This test has been repeated in two porcine eyes with a total of 58
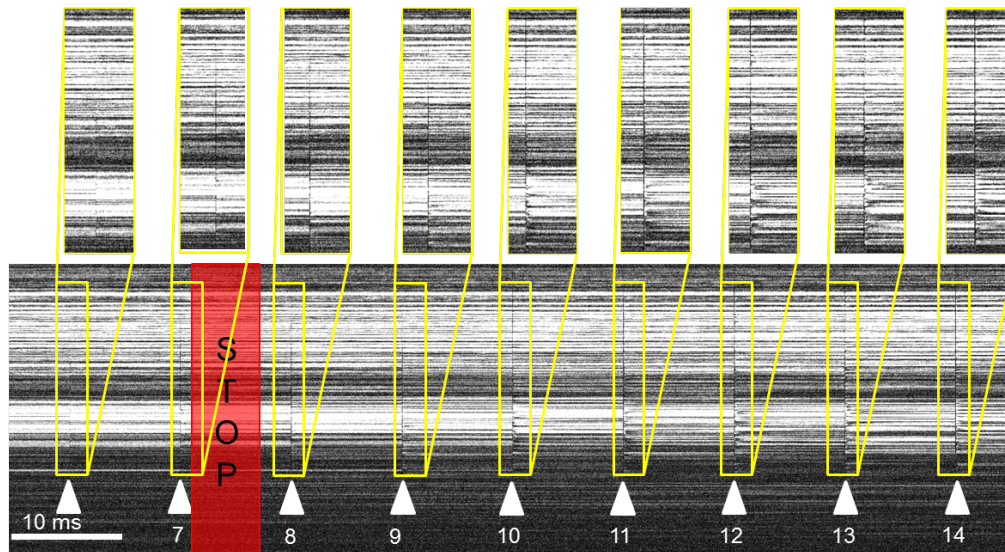
Fig. 7. Numbering on the horizontal-axis correspond to the laser pulse applied in ramp-mode where the pulse events are indicated by white arrows. Signal washouts in the M-scan were becoming more apparent with each pulse and thus with increasing pulse energy. On the zoomed-out signal washouts, this effect is observable. During automated dose-control, the first signal washout would be detected (in this case it is number 7) and the laser would stop shooting, indicated by the red marker. Pulse 8 to 14 would not be fired.

included treatment spots. For every spot, there was an M-scan with a visible signal loss before the treatment was stopped. Under the microscope, 55 out of the 58 spots were identified as lesions and therefore as a successful treatment, which hence yields an accuracy of almost 95%. Exposures stopped at the threshold did not cause visual alterations of the morphology viewed from the retinal side. This very promising result makes us confident that following our proposed treatment protocol will indeed dependably control the necessary pulse energy for an optimal SRT of individual patients.

Conclusion

Findings from this study successfully demonstrate the potential of OCT utilization for an automated dose-control in SRT. It can be established as a safe method of treatment for retinal diseases by using its full potential with an optimum combination and interaction between treatment system and monitoring modality, including eye motion tracking and offline treatment planning in a clinical environment.

Although this study has not yet implemented a complete automated system it has shown the proof of concept for a device where the ophthalmologist chooses the location of treatment and manually initiates a ramped sequence of pulses, similar to established solutions. Collinear coupled OCT acquired data would be processed in real time, and as soon as a first signal washout is detected, the treatment laser stops automatically at a dose significantly below the local, individual safety threshold. Latter can be preset by the clinician together with an absolute maximum value to avoid undesired photocoagulation. For optimal treatment the therapeutic window, defined as the ratio between the ophthalmologic and the angiographic ED_{50}, can be set to a predefined value, such as 1.7 [19]. This intentionally pre-set overexposure would reduce the necessity for re-treatment, while keeping the collateral damage limited.

We, and other groups as well, are certain that laser treatment is a very promising therapy for retinal diseases in the future [55].

Funding

Acknowledgments

Disclosures

The authors declare that there are no conflicts of interest related to this article.